Stephan E. Maier, MD, PhD
Peter Bogner, MD, PhD
Gabor Bajzik, MD
Hatsuho Mamata, MD
Yoshiaki Mamata, MD
Imre Repa, MD
Ferenc A. Jolesz, MD
Robert V. Mulkern, PhD

Index terms:
Brain, edema, 10.86
Brain, gray matter
Brain, white matter
Brain neoplasms, MR, 10.121411, 10.12143
Magnetic resonance (MR), contrast enhancement, 10.12143
Magnetic resonance (MR), diffusion study, 10.12144
Magnetic resonance (MR), tissue characterization

Radiology 2001; 219:842–849

Abbreviations:
ADC = apparent diffusion coefficient
A_1 = signal amplitude for ADC_1
A_2 = signal amplitude for ADC_2
ROI = region of interest

[1] From the Departments of Radiology, Brigham and Women's Hospital (S.E.M., H.M., Y.M., F.A.J.) and Children's Hospital (R.V.M.), Harvard Medical School, 75 Francis St, Boston, MA 02115; and the Diagnostics Center, Pannon University of Agriculture, Kaposvar, Hungary (P.B., G.B., I.R.). Received June 27, 2000; revision requested August 7; revision received September 6; accepted September 11. S.E.M. supported by grants from the Whitaker Foundation and the National Institutes of Health (NIH 1R01 NS39335-01A1). P.B. supported by Hungarian Scientific Research Fund (OTKA grants F 016343, T 034200). **Address correspondence to** S.E.M. (e-mail: *stephan@bwh.harvard.edu*).

Author contributions:
Guarantor of integrity of entire study, S.E.M.; study concepts, S.E.M., R.V.M.; study design, S.E.M., P.B.; definition of intellectual content and editing, S.E.M., P.B., R.V.M.; literature research, P.B.; clinical studies, P.B.; data acquisition, P.B., S.E.M.; data analysis, P.B., G.B., S.E.M., H.M., Y.M.; statistical analysis, S.E.M., P.B., G.B., H.M., Y.M.; manuscript preparation, S.E.M., P.B.; manuscript review, R.V.M., F.A.J., I.R.; manuscript final version approval, S.E.M., R.V.M.

Normal Brain and Brain Tumor: Multicomponent Apparent Diffusion Coefficient Line Scan Imaging[1]

Magnetic resonance line scan diffusion imaging of the brain, with diffusion weighting between 5 and 5,000 sec/mm^2, was performed in healthy subjects and patients with a 1.5-T machine. For each voxel, biexponential signal decay fits produced two apparent diffusion constants and respective signal amplitudes. Images based on these parameters show potential for use in the differentiation of gray and white matter, edema, and tumor.

Tissue characterization is a basic issue in magnetic resonance (MR) imaging. In fact, the concept of distinguishing normal and tumor tissue with MR imaging goes back to the observation of Damadian (1), who described substantial differences in T1 and T2 between normal and cancerous tissue. Since then, methods to obtain T1- or T2-weighted images have improved dramatically, and considerable experience has been gained with the in vivo application of these methods with the use of contrast agents. Nevertheless, determination of the tumor margin solely on the basis of contrast enhancement on T1- or T2-weighted images is not successful in every case (2,3).

In several recent publications (4–9), diffusion-weighted imaging has been proposed as a novel mechanism for producing contrast in the demarcation of different cerebral tumors. Apparent diffusion coefficient (ADC) maps of brain tumors seem also to provide useful information about structural details of tumors (5,7,8). According to these reports, peritumoral edema and solid enhanced, solid necrotic nonenhanced, and cystic parts can be recognized on ADC maps. Diffusion tensor imaging adds information about the directional dependence of molecular diffusion that may also be helpful in the demarcation of tumor margins (10). Nevertheless, any of these new diffusion imaging methods used with contrast material–enhanced relaxation-weighted imaging fails to be specific enough in every case (5,6).

Routine diffusion imaging of the brain generally involves the use of *b* factors within the range of 0 to 1,000 sec/mm^2. ADC maps are then generated, based on the assumption that the relationship between the MR signal and *b* factor is monoexponential. Recently, however, it was shown (11) that for rat brain, the signal decay with *b* factors in an extended range of up to 10,000 sec/mm^2 is better described with a biexponential curve. Similar findings were made in human brain by using multiple *b* factors of up to 6,000 sec/mm^2 (12). Both studies lack the anatomic details needed for clinical application, since diffusion was measured only within a localized volume (11) or along a column (12).

In the present study, our goal was to obtain diffusion-weighted images of the human brain with *b* factors ranging from 5 to 5,000 sec/mm^2. Biexponential fits were applied to the measured signal of each voxel. With the four parameters that describe the biexponential fit, we attempted to characterize normal white and gray matter, edematous white matter, and brain tumors.

Materials and Methods

Healthy Subjects and Patients

This study included two healthy subjects and 15 patients, including 14 patients with brain tumors (seven men, seven women; age range, 33–79 years;

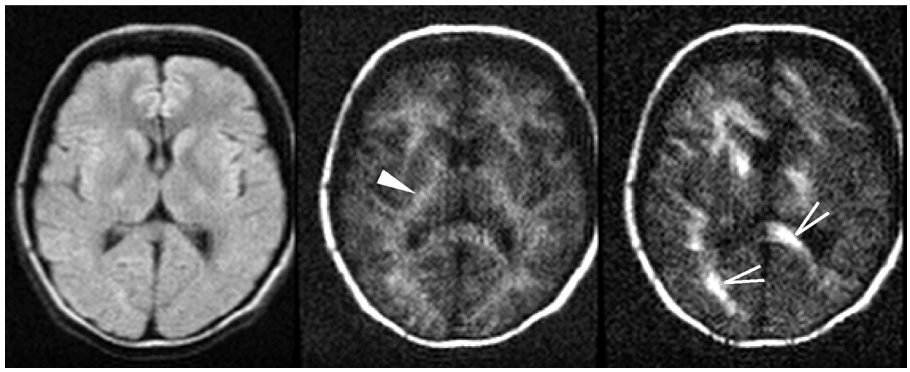

Figure 1. Transverse line scan diffusion-weighted MR images of a normal brain (3,600/94; 128 × 96 matrix; field of view, 220 × 165 mm; section thickness, 6 mm). The image on the left is a trace diffusion-weighted image with a typical *b* factor of 1,080 sec/mm^2. The other two images were obtained with very high diffusion weighting of 5,000 sec/mm^2: The image in the middle is trace diffusion weighted, whereas the image on the right is monodirectional diffusion encoded in a (1,1,1) gradient configuration. With very high diffusion weighting, white matter tracts are enhanced, for example, the internal capsule (solid arrowhead). On the monodirectional diffusion-encoded image, anisotropic diffusion leads to selective enhancement of white matter tracts, for example, the right optical tract and left half of corpus callosum (open arrowheads), that are not aligned with the diffusion encoding direction.

mean age, 56 years) and one patient with subacute stroke. In the healthy subjects, brain images obtained for localization revealed no abnormalities. The patients with tumor included two with astrocytoma, eight with glioblastoma, and four with metastases. All diagnoses were confirmed at preoperative biopsy or surgical resection. All studies in healthy subjects and patients were performed within the guidelines of the institutional internal review board. Informed consent was obtained from healthy subjects, patients, or their authorized representatives.

MR Diffusion Imaging

Each patient underwent the routine clinical imaging protocol. This protocol included T2-weighted (3,000–3,600/80–98, repetition time msec/echo time msec; field of view, 220–240 × 220–240 mm; section thickness, 3–5 mm) and T1-weighted (500–700/14–25; field of view, 220–240 × 220–240 mm; section thickness, 3–5 mm) spin-echo sequences before and after contrast enhancement (Magnevist [gadopentetate dimeglumine]; Berlex Laboratories, Wayne, NJ; 0.2 mL per kilogram of body weight administered in the cubital vein) to localize the tumor mass and other pathologic details. For that obvious reason, in most cases diffusion imaging was performed only after the administration of contrast material. In four patients, the section for diffusion imaging of tumor tissue was determined with nonenhanced images, and diffusion imaging was performed prior to the administration of contrast agent. One patient with tumor underwent diffusion imaging before and after the administration of contrast material.

Diffusion-weighted images with a wide range of *b* factors were obtained with line scan diffusion imaging. Aspects of the MR physics and the feasibility of this single-shot column-sampling technique have been presented (13). Patient studies with line scan diffusion imaging (14,15) have demonstrated the usefulness of this technique for conventional diffusion imaging. The line scan diffusion sequence was implemented by using a 1.5-T whole-body system (Signa Echospeed; GE Medical Systems, Milwaukee, Wis) with version 5.7 software. The maximum gradient strength was 22 mT/m. The standard birdcage coil was used, and neither cardiac gating nor head restraints were used.

Images were acquired with a rectangular field of view of 220 × 165 mm and a matrix size of 64 × 48 or 126 × 96 columns. The effective section thickness (13) was set at 6.0–7.3 mm. The receiver bandwidth was set at 6.25 kHz, which was found to be the best compromise in view of the decreased signal-to-noise ratio at higher bandwidths and the augmented image distortions caused by field inhomogeneities or chemical shifting at lower bandwidths. Sixteen images with linearly increasing diffusion weighting between 5 and 5,000 sec/mm^2 were acquired.

For patient imaging, diffusion was measured along only a single direction, in a (1,1,1) gradient configuration to achieve maximal diffusion encoding with a minimal echo time of 94 msec. A *b* factor of 5,000 sec/mm^2 was attained with trapezoidal gradient pulses of 36.2 mT/m amplitude, 40-msec pulse duration (δ), and 46 msec between the onset of the first and second gradient pulses (Δ). In healthy subjects, data along six non-colinear directions were collected with the tensor configuration described by Basser and Pierpaoli (16) by using an echo time of 107 msec. The repetition time and effective repetition time (13) were 204 and 2,040–3,600 msec, respectively; the total imaging time was 3 minutes per section (one diffusion direction with 16 *b* factors). Shorter repetition and imaging times would have been possible had gradient heating not been a concern.

Data Analysis

Data analysis was performed offline at workstations (Sun Microsystems, Mountain View, Calif) by using MATLAB software (Math Works, Natick, Mass). A nonlinear least-squares Marquardt algorithm was used for each pixel to fit brain signal intensity decay S with diffusion-weighting b to a biexponential function of the following form: $S = A_1 \exp(-\mathrm{ADC}_1 b) + A_2 \exp(-\mathrm{ADC}_2 b)$, where ADC_1 and ADC_2 are the ADCs, with the signal amplitudes for ADC_1 (A_1) and ADC_2 (A_2).

Data points were included in the fit only if their signal exceeded three times the noise baseline, defined by the mean signal intensity in the four corners of the image. Changes in the calibration of the MR apparatus do not permit a direct comparison among biexponential signal amplitudes measured during different acquisitions. We therefore calculated the relative fraction of the biexponential signal amplitude of the slow diffusing component as follows: $A_2/(A_1 + A_2)$. Preliminary experiments with a phantom that simulates the geometry and load of a human head (head SNR phantom model 46-287900G3; GE Medical Systems) showed that within a 170-mm diameter the signal variations are 4.4%. We considered these variations small enough to permit normalization of individual tissue values (A_{1T} and A_{2T}) with individual white matter values (A_{1W} and A_{2W}) measured at a different location.

Maps of the fit parameters were used for region-of-interest (ROI) analysis with dedicated image-analysis software (XPHASE) developed at our institution. With this program, the contour drawing process can be simultaneously controlled on different image backgrounds (eg, T1-weighted, T2-

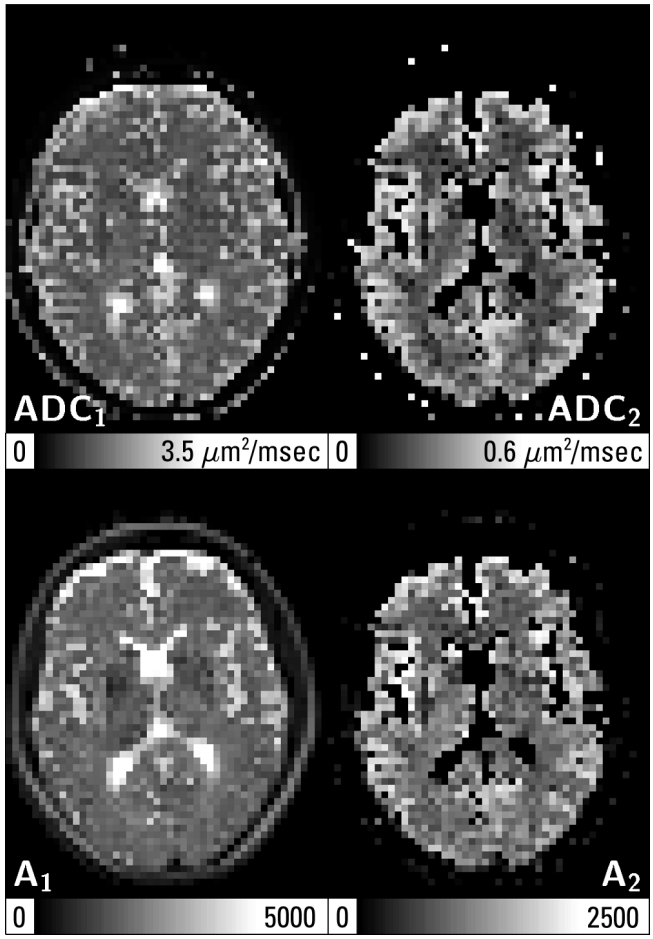

Figure 2. Images of the parameters ADC_1, ADC_2, A_1, and A_2 generated from biexponential signal analysis. Data were obtained from transverse MR images (2,380/107; 64 × 48 matrix; field of view, 220 × 165 mm; section thickness, 7.3 mm; *b* factor, 5–5,000 sec/mm^2; tensor configuration [16]) in a healthy subject. The annotation of the gray scale for the A_1 and A_2 maps is in arbitrary units.

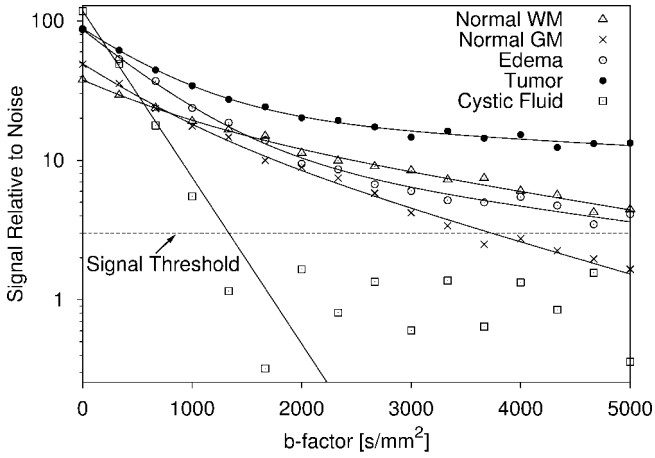

Figure 3. Logarithmic plot of MR signal intensity versus *b* factor for individual pixels in areas of normal white matter (*WM*) and gray matter (*GM*), edema, tumor, and cystic fluid. Points below the signal threshold were not included in the fit calculations (see Materials and Methods section). Biexponential fits of the data points are shown for tissues. For the cystic fluid, data points for a *b* factor of more than 1,000 sec/mm^2 are below the signal threshold, and the best fit is monoexponential. The elevated amplitude of the slow-diffusing component in tumor tissue is well discernible.

weighted, and ADC). ROIs were drawn manually by two of the authors (P.B., G.B.) in consensus.

The ROI for tumor tissue was defined according to contrast enhancement on the conventional T1-weighted images. Separate ROIs were drawn for cystic parts of tumor lesions. The ROI for peritumoral edema was defined with the use of nonenhanced T2-weighted images and contrast-enhanced T1-weighted images. Nonpathologic periventricular white matter areas were selected as a healthy control. To reduce the influence of directional diffusion, the mean value of two independent and large white matter ROIs was used. Gray matter values were determined in the cortex. In all cases, ROI size and placement were selected so that bordering tissues of ambiguous origin were excluded as much as possible. Moreover, to avoid partial volume effects in the ROI analysis of the relatively thick sections used at line scan diffusion imaging, considerable effort was made to determine that the tissue of interest was also present on neighboring sections of the conventional images.

ROI sizes for tumors ranged between 5 and 29 pixels (mean, 15.4 pixels or 182 mm^2). All other ROIs were, on average, larger; that is, there were 27.7 pixels for cysts, 24.6 pixels for peritumoral edema, 62.7 pixels for gray matter, and 25.4 pixels for gray matter. Significant differences among mean ROI values were verified with a two-sided Student *t* test, with *P* values less than .05 considered to indicate a significant difference.

Results

Figure 1 shows a diffusion-weighted image of the brain of a healthy subject with a *b* factor typically used for routine clinical examination, along with a diffusion-weighted image acquired with a *b* factor of 5,000 sec/mm^2, that is, a higher-than-usual *b* factor. Figure 2 shows maps of ADC_1, ADC_2, A_1, and A_2, computed from an image obtained with a wide range of *b* factors in another healthy subject. On the ADC_2 and A_2 maps, values in the ventricles were zero, since the signal decay in cerebrospinal fluid is monoexponential.

Moreover, differences between white and gray matter were also evident on the maps of the slow diffusing component. Figure 3 shows typical signal decays in individual pixels and the respective fits for normal white and gray matter, edematous white matter, tumor tissue, and cystic fluid, as determined from a study in a patient with tumor. Only by grossly exceeding the clinically used *b* factor range of 0–1,000 sec/mm^2 did the biexponential nature of the signal decay for white and gray matter, edema, and tumor become apparent. If the decay were monoexponential, the signal decay on a logarithmic plot would follow a straight line. Noise cannot explain the multiexponential decay, since, except for that of cystic fluid, all MR signal amplitudes were well above the noise threshold up to a *b* factor of 5,000 sec/mm^2.

Attempts to fit brain signal decay curves, except for those of the cerebrospinal fluid and cystic parts of the tumor

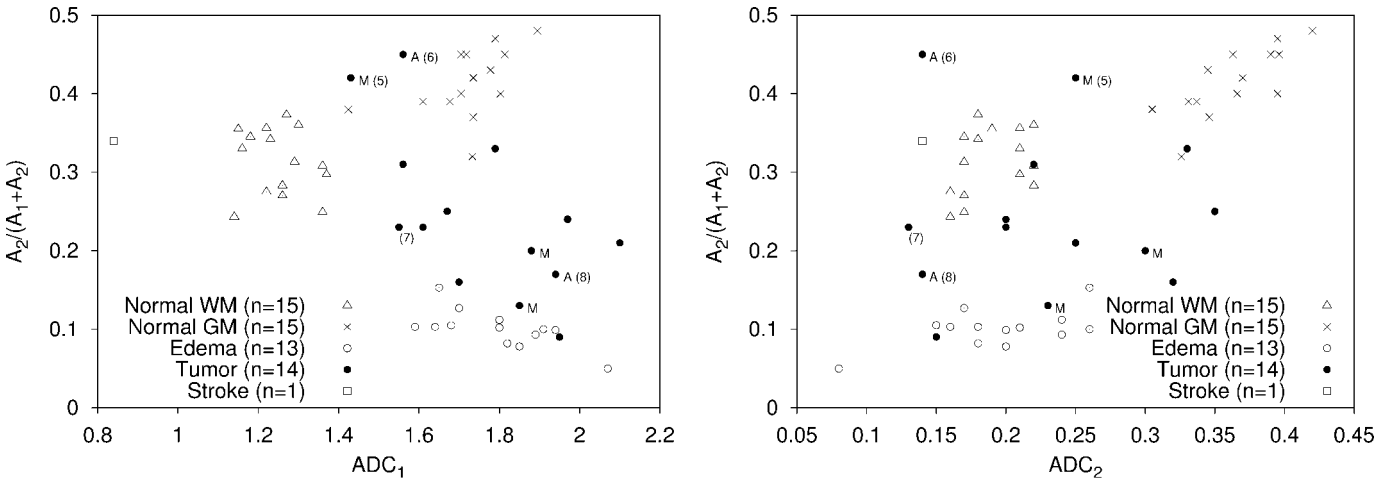

a. **b.**

Figure 4. Scatterplots of the relative biexponential signal amplitude fraction $A_2/(A_1 + A_2)$ versus **(a)** ADC_1 and **(b)** ADC_2 ROI values (in square micrometers per millisecond). Numbers in parentheses indicate the number of the figure in which images of the particular case are presented. Differentiation of astrocytoma (*A*) and metastatic tumors (*M*) on the basis of these two diffusion parameters seems difficult, although more samples are needed to fully address this issue. *GM* = gray matter, *WM* = white matter.

lesions, with monoexponential functions led to χ^2 values that were more than an order of magnitude larger than those obtained from biexponential fits. Triexponential fitting functions yielded unstable parameters, with no significant decrease in χ^2 values compared with those obtained from biexponential fits.

Mean ROI values and SDs of the fast-diffusing component (ADC_1), the slow-diffusing component (ADC_2), and the relative fraction of the slow-diffusing component are summarized in the Table. For each cystic lesion, only one ADC value was calculated from the slope of the monoexponential line fit to the logarithm of the MR signal intensity. The measured ADC for cystic lesions was, on average, comparable with the ADC of water at 37°C (3.0 μm^2/msec [17]). The biexponential signal intensity ratio between different tissues and normal white matter are listed in the Table. Moreover, to provide a quantitative expression of the appearance of the pathologic areas on the diffusion-weighted images, corresponding ratios of the MR signal intensities at low, high, and very high diffusion weighting are also given in the Table. The data in one of the patients with a metastasis were not suitable for analysis because of severe motion artifacts. In one of the patients with glioblastoma, peritumoral edema was not depicted in the selected section.

Mean Biexponential Diffusion Parameters, Biexponential Signal Amplitude Ratios, and Signal Intensity Ratios

A: Biexponential Diffusion Parameters

Tissue	ADC_1 (μm^2/msec)	ADC_2 (μm^2/msec)	$A_2/(A_1 + A_2)$*
White matter (n = 15)	1.25 (0.08)	0.19 (0.02)	0.31 (0.04)
Gray matter (n = 15)	1.71 (0.12)	0.37 (0.04)	0.42 (0.05)
Edema (n = 13)	1.80 (0.14)†	0.20 (0.05)†	0.10 (0.02)‡
Tumor (n = 14)	1.75 (0.20)	0.23 (0.07)	0.24 (0.10)
Cyst (n = 5)	2.75 (0.19)	Not applicable	Not applicable
Stroke (n = 1)	0.84	0.14	0.34

B: Biexponential Signal Amplitude Ratios between Tissue and Normal White Matter

Tissue	A_{1T}/A_{1W}§	A_{2T}/A_{2W}§
Gray matter (n = 15)	0.96 (0.10)	1.55 (0.21)
Edema (n = 13)	2.78 (0.26)‖	0.73 (0.25)‡
Tumor (n = 14)	2.18 (0.57)	1.53 (0.68)
Cyst (n = 4)	4.45 (0.59)	Not applicable

C: Signal Intensity Ratios between Tissue and Normal White Matter

Tissue	b = 5 sec/mm²	b = 1,004 sec/mm²	b = 5,000 sec/mm²
Gray matter (n = 15)	1.12 (0.06)	0.98 (0.08)	0.71 (0.23)
Edema (n = 13)	1.95 (0.56)†	1.04 (0.17)#	0.64 (0.20)#
Tumor (n = 14)	1.87 (0.37)	1.29 (0.37)	1.29 (0.95)
Cyst (n = 4)	2.79 (0.63)	0.43 (0.14)	Not applicable

Note.—Data in parentheses are the SDs.
* *A* is signal amplitude.
† Difference between this value and that of tumor was not significant; $P > .05$.
‡ Difference between this value and that of tumor was significant; $P < .001$.
§ *A* is signal amplitude, *T* is tissue, and *W* is white matter.
‖ Difference between this value and that of tumor was significant; $P < .01$.
Difference between this value and that of tumor was significant; $P < .05$.

The scatterplot in Figure 4 presents the relative A_2 fraction versus ADC_1 and ADC_2 data of individual ROI measurements. Evidently, both the A_2 fraction and the ADC_1 value alone permit a clear separation between normal white matter and edematous white matter. None of these parameters by itself is sufficient to allow separation of tumor from brain tissues. Together, the A_2 fraction, ADC_1, and ADC_2 permit the separation between tumor and other brain tissues in about

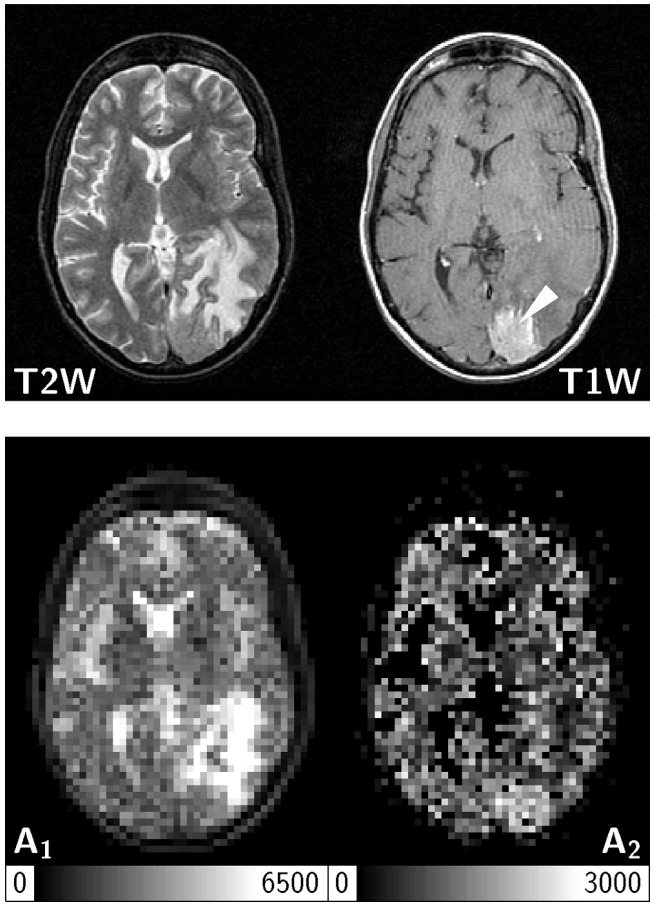

Figure 5. Transverse MR images of a breast adenocarcinoma metastasis in the left occipital lobe. The extent of edema is seen on the T2-weighted (*T2W*) spin-echo image (3,000/80; field of view, 240 × 240 mm; section thickness, 3 mm). The tumor lesion (arrowhead) is enhanced on the T1-weighted (*T1W*) contrast-enhanced spin-echo image (700/14; field of view, 240 × 240 mm; section thickness, 3 mm). On the T2-weighted image, the same area appears slightly brighter (38% higher signal intensity) than the normal white matter on the opposite side. The A_1 map that was calculated from diffusion-weighted images with a wide *b* factor range obtained after the administration of contrast material (2,040/94; 64 × 48 matrix; field of view, 220 × 165 mm; section thickness, 7.3 mm; *b* factor, 5–5,000 sec/mm^2) also shows the edema. The A_2 map depicts the tumor lesion, with a size and location comparable to those on the contrast-enhanced T1-weighted image.

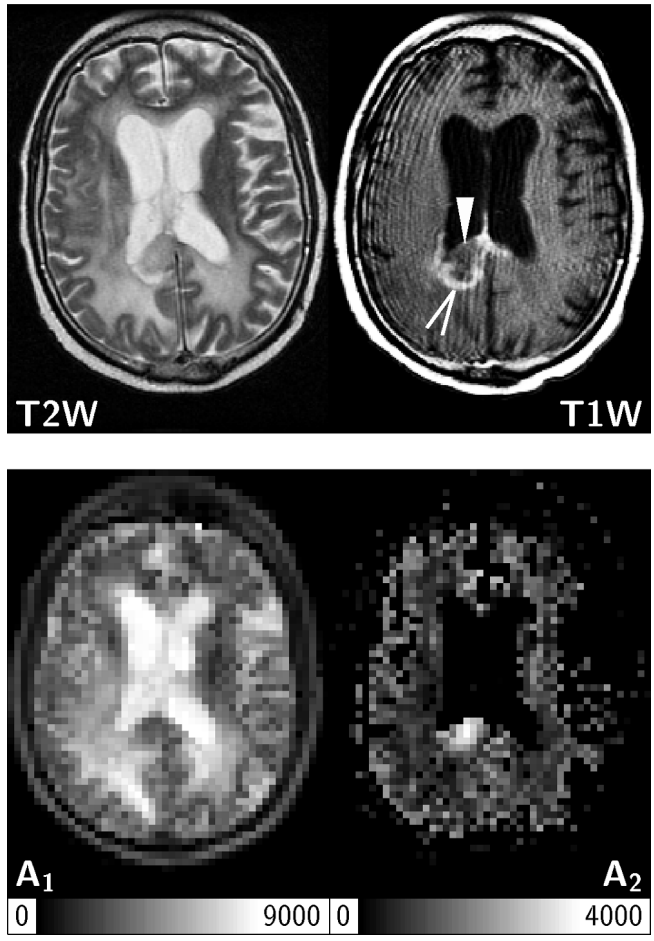

Figure 6. Transverse MR images of an anaplastic astrocytoma localized in the splenium of the corpus callosum. The extent of edema is seen on the T2-weighted (*T2W*) spin-echo image (3,000/98; field of view, 220 × 220 mm; section thickness, 5 mm) and on the A_1 map that was calculated from images obtained with a wide *b* factor range prior to the administration of contrast material (2,040/94; 64 × 48 matrix; field of view, 220 × 165 mm; section thickness, 7.3 mm; *b* factor, 5–5,000 sec/mm^2). The border (open arrowhead) of the tumor lesion is enhanced on the T1-weighted (*T1W*) contrast-enhanced spin-echo image (600/25; field of view, 220 × 220 mm; section thickness, 5 mm). The solid part of the lesion (solid arrowhead) shows no enhancement on the T1-weighted image but appears bright on the A_2 map.

two-thirds of patients. However, on three of the 14 images in patients with tumor, tumor values were not different from edema or gray matter values.

Despite limited resolution and a relatively poor signal-to-noise ratio, the calculated maps showed a genuine separation of tumor in most cases; that is, the tumor area was clearly separate from the peritumoral edema and normal white matter. The cystic components of tumors were easily recognized; however, no attempt was made to distinguish necrotic and solid parts or other minute details of tumor types.

Figure 5 shows images of a metastasis of a breast adenocarcinoma in the left occipital lobe. On the T2-weighted image, the tumor appears to have a signal intensity that is slightly higher than that of normal white matter. The lesion is surrounded by edema that extends to the thalamus and the dorsal limb of the external capsule. The A_1 map, which represents the biexponential signal amplitude of the fast-diffusing component of tissue water, clearly delineates the edema without tumor. The tumor is seen separately on the A_2 map that represents the biexponential signal amplitude of the slow-diffusing component.

The images in Figure 6 are from a patient with an anaplastic astrocytoma in the splenium of the corpus callosum. The examination was performed as a control examination in an ongoing radiation therapy program. The diffuse high signal intensity in the periventricular white matter on the T2-weighted image may, therefore, be a side effect of this therapy. A congruent diffuse high-signal-intensity pattern is seen on the A_1 map. Moreover, similar to the case in Figure 5, the tumor lesion, as defined by the contrast-enhanced T1-weighted image, is not part of the high-signal-intensity area seen on the A_1 map. The A_2 map, however, provides good depiction of the tumor, with high signal in-

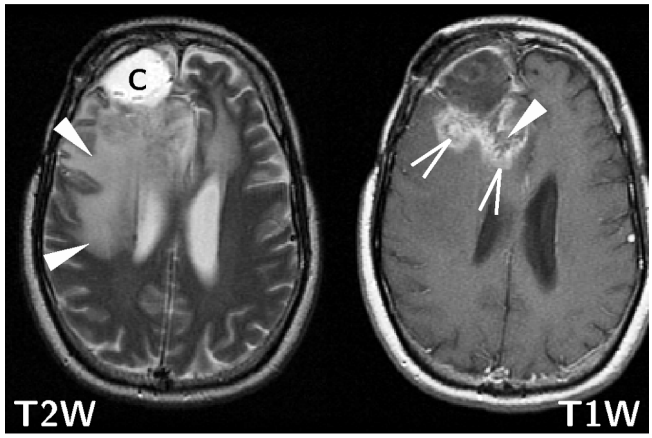

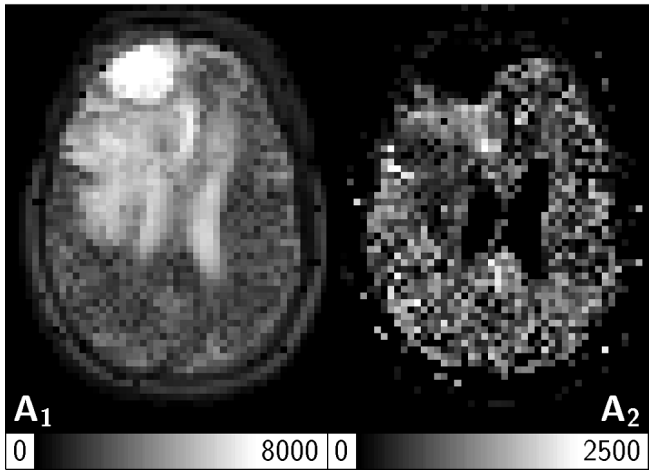

Figure 7. Transverse MR images of a frontal glioblastoma with a postoperative cyst. The edema (solid arrowheads) and cyst (*C*) are enhanced on the T2-weighted (*T2W*) spin-echo image (3,600/98; field of view, 220 × 220 mm; section thickness, 5 mm) and the A_1 map. The T1-weighted (*T1W*) contrast-enhanced spin-echo image (600/25; field of view, 220 × 220 mm; section thickness, 5 mm) predominantly shows the margins (open arrowheads) and not the solid part (solid arrowhead) of the tumor. However, the A_2 map that was calculated from images obtained with a wide *b* factor range (2,040/94; 64 × 48 matrix, field of view, 220 × 165 mm; section thickness, 7.3 mm; *b* factor, 5–5,000 sec/mm^2) shows the solid part of the tumor. The area of edema appears remarkably dark on the A_2 map.

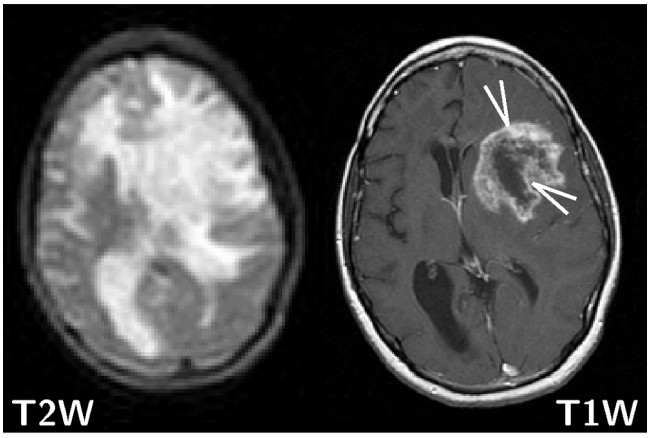

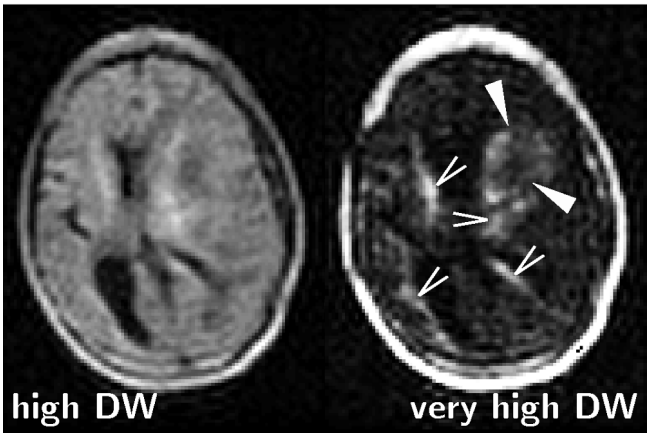

Figure 8. Transverse MR images of an astrocytoma with edema. The line scan images (2,040/94; 64 × 48 matrix; field of view, 220 × 165 mm; and section thickness, 7.3 mm) were obtained prior to the administration of contrast material. Edema and tumor are enhanced on the T2-weighted (*T2W*) line scan spin-echo image (*b* factor, 5 sec/mm^2). The ventricular system appears to be compressed on one side and enlarged on the other. The tumor lesion margins (open arrowheads on upper right image) are depicted on the T1-weighted (*T1W*) contrast-enhanced spin-echo image (500/25; field of view, 220 × 220 mm; section thickness, 5 mm). On the diffusion-weighted (*DW*) image obtained with a conventional *b* factor of 1,004 sec/mm^2 (high diffusion weighting), no signal intensity enhancement is seen in the areas of edema and tumor, whereas on the image obtained with a *b* factor of 5,000 sec/mm^2 (very high diffusion weighting), the tumor (solid arrowheads) is enhanced. Also enhanced are white matter tracts (open arrowheads on lower right image) that are not aligned with the diffusion encoding direction (compare with Fig 1).

tensity and excellent contrast between tumor and surrounding white matter.

Figure 7 shows a case of postoperative glioblastoma. The lesion in the right frontal brain includes a cyst and a contrast-enhanced solid part dorsal to the cyst. Substantial peritumoral edema is present, reaching as far as the central sulcus. Note that unlike the cases in Figures 5 and 6, tumor tissue is also enhanced on the T2-weighted image and the A_1 map. The images of another case of astrocytoma shown in Figure 8 demonstrate that normal diffusion weighting will not cause enhancement in solid tumor structures. However, the elevated biexponential signal amplitude of the slow-diffusing component produces selective signal enhancement in areas of tumor tissue on the image with very high diffusion weighting.

Discussion

It has been demonstrated that diffusion-weighted imaging with a *b* factor range wider than that typically used can be performed in healthy subjects and patients. The line scan diffusion imaging technique appears to be suitable for the acquisition of images free of motion artifacts, even with very high *b* factors of up to 5,000 sec/mm^2. The fact that imaging with very high diffusion weighting failed in only one of 15 patients is evidence of a remarkable degree of robustness. Single-shot diffusion-weighted echo-planar imaging (18), which was not available with our MR system at the time of this study, would have been equally insensitive to motion. Moreover, with echo-planar imaging, data from more than one section could have been obtained without increasing the imaging time.

On the other hand, in areas near large

bone structures, the sensitivity of single-shot echo-planar imaging to susceptibility variations and chemical shifting can, with inadequate shimming, result in ghosting artifacts, image distortions, or complete signal loss, whereas images obtained with line scan diffusion imaging do not show such artifacts (14,15). In addition, eddy currents that are caused by the application of the diffusion encoding gradients can generate distortion artifacts (19). One would expect that these distortion artifacts increase with higher *b* factors. With line scan diffusion imaging, however, no distortions were observed, even with the highest *b* factors.

These findings, in agreement with those of earlier reports (11,12), revealed that biexponential fits better describe diffusion-related signal loss in the brain. The deviation from a purely monoexponential model that becomes evident as the diffusion encoding is extended beyond the normal range should not be confounded with effects that arise from microcirculation (20,21). Signal loss due to microcirculation is observed only with *b* factors of less than 300 sec/mm^2 and therefore cannot account for the deviations measured in various tissues. A reanalysis of the data without use of the lowest *b* factor (ie, only 15 *b* factors between 338 and 5,000 sec/mm^2) revealed the same biexponential behavior. The normal human white matter parameters observed in the current study are in good agreement with those of an earlier study (12) in which a considerably higher number of *b* factors over a slightly larger range were used. Limitations in the interpretation of the slow ADC component as intracellular water and the fast ADC component as extracellular water, including a discrepancy between the ADC component volume fractions and reported values of intracellular and extracellular water volume fractions in brain, were discussed by Niendorf et al (11).

The novelty of this study, besides the acquisition of these fit parameters in image formats, is the observation of biexponential diffusion in pathologic brain tissues. Moreover, the four parameters that describe the biexponential fit seem to permit the distinction among the various tissues. In normal cortical gray matter compared with normal white matter, all parameters except the biexponential signal amplitude A_2 were strongly elevated. The low spatial resolution of the collected data may have resulted in a contamination of the measured signal with cerebrospinal fluid signal. This signal contamination would primarily affect the measurement of the fast-diffusing component, since the monoexponential diffusion constant of cerebrospinal fluid is relatively high. In subacutely infarcted tissue, a lower ADC for the fast-diffusing component (Table) is expected, since it is known from conventional diffusion imaging that diffusion is reduced (22). In the present study, the ADC of the slow-diffusing component was also reduced. This observation, however, is not well corroborated, since only one patient with stroke participated in the study.

Characteristic changes in biexponential diffusion parameters, which remain to be explained, were observed in peritumoral edema and tumor tissue; compared with the value in white matter, the ADC_1 value increased by almost 50%. The A_1 value increased by 178% in edema and 118% in tumor tissue. While there were only minimal changes in the ADC value of the slow-diffusing component, the biexponential signal amplitude A_2 decreased in peritumoral edematous white matter, whereas it increased in tumor tissue. We do not have an explanation for the contrary behavior of the biexponential signal amplitude of the slow-diffusing component in the two tissues, since the exact nature of the biexponential signal attenuation is not known. The amplitude of each diffusion constant is influenced by the spin density and relaxation time of each observed component. Since spin density and the relaxation times of the components are not necessarily the same, imaging protocols with different settings of the repetition and/or echo time may yield different amplitude values.

In another study (23), however, we found no statistically significant differences in T1 relaxation. It can be speculated that the slow-diffusing component is determined by the concentration of water-binding macromolecules, cellular size, and tissue architecture (tortuosity) (24–28), that is, factors that are indeed different among the investigated tissues. Thus ADC_1, ADC_2, and the biexponential signal amplitudes A_1 and A_2 permit the separation of the various tissues.

Changes in tumor tissue appear to be more variable, which most likely reflects the fact that tumors do not represent a single type of tissue. From the limited number of different tumor types studied with this technique to date, correlations between histologic type and biexponential diffusion parameters cannot be established. Cystic regions are easily distinguished by their monoexponential diffusion and high ADC.

Another limitation of the current study is the monodirectional diffusion encoding used for patient imaging. As pointed out in the Data Analysis section, to reduce the potential error in white matter tracts where restricted diffusion is most likely to be present, the mean value of two independent and large white matter ROIs was used. For each case (eg, Fig 6), we also verified that the observed tumor enhancement was not due to restricted diffusion in a white matter tract.

Diffusion-based tissue differentiation does not depend on the use of contrast agents, since the diffusion-weighted images are only minimally T1-weighted (effective repetition time, 2,040 msec) (29). The tumor-tissue contrast generated on multicomponent ADC maps is different from the enhancement produced by paramagnetic contrast agents. The contrast agents in use are not specific to tumor tissue, but rather, they enhance areas where the blood-brain barrier has become permeable due to neoplastic growth, surgical procedures, or radiation therapy (2,3). Moreover, not all tumor types enhance with the use of contrast agents. On multicomponent ADC maps, on the other hand, as demonstrated in Figures 6 and 7, enhancement occurs in the solid part of the tumor.

Diffusion-weighted imaging has been previously evaluated (5–7) in the characterization of brain tumors and associated pathologic structures. With this study, we demonstrated that only limited information is gained from diffusion imaging in the normal *b* factor range (Fig 3). With very high *b* factors, however, the signal in tumor tissue is elevated in comparison with that of surrounding edema and normal white matter; the elevated signal is due to the higher biexponential signal amplitude of the slow-diffusing component in tumor tissue. The data in the Table and the diffusion-weighted images in Figure 8 reiterate this observation: With low diffusion weighting, peritumoral edema and tumor tissue are enhanced; at high diffusion weighting (around 1,000 sec/mm^2), the contrast among the different tissues is minimal; and at very high diffusion weighting, tumor tissue is selectively enhanced.

From the equation in the Materials and Methods section, it follows that for *b* equal to 0, the measured signal equals A_1 plus A_2. At very high diffusion weighting, the signal is dominated by the second diffusion component, that is, $S \approx A_2 \exp(-ADC_2 b)$. Consequently, for white matter, edema, and tumor, where ADC_2 is similar (Fig 4b, Table), images

obtained with very high diffusion imaging may be considered A_2-weighted. Thus, for routine diagnostic imaging, it may be sufficient to acquire only one diffusion-weighted image with very high diffusion weighting. Signal averaging by using different diffusion encoding directions could then be performed to overcome a poor signal-to-noise ratio and limited spatial resolution. Trace diffusion weighting would be necessary to eliminate selective enhancement of white matter tracts (Fig 8), which could be misinterpreted as lesions.

In summary, we investigated a method for tissue characterization with multiexponential analysis of the diffusion-attenuated signal. We examined brain tumors, and our results indicated that the calculated images of slow- and fast-diffusing components helped distinguish edema and tumor tissue in a number of cases. Provided that more experience is gained with different tumor types, the technique could potentially be used without paramagnetic contrast agents for tumor localization. Clearly, further experiments are needed to reveal the biophysical basis of the described phenomenon and to optimize the method for routine clinical diagnosis.

References

1. Damadian R. Tumor detection by nuclear magnetic resonance. Science 1971; 171: 1151–1153.
2. Hasso AN, Kortman KE, Bradley WG. Supratentorial neoplasms. In: Stark DD, Bradley WG Jr, eds. Magnetic resonance imaging. 2nd ed. Vol 1. St Louis, Mo: Mosby–Year Book, 1992; 770–817.
3. Hicks RJ. Supratentorial brain tumors. In: Edelman RR, Hesselink JR, Zlatkin MB, eds. Clinical magnetic resonance imaging. 2nd ed. Vol 1. Philadelphia, Pa: Saunders, 1996; 533–556.
4. Eis M, Els T, Hoehn-Berlage M, Hossman KA. Quantitative diffusion MR imaging of cerebral tumor and edema. Acta Neurochir Suppl (Wien) 1994; 60:344–346.
5. Krabbe K, Gideon P, Wagn P, Hansen U, Thomsen C, Madsen F. MR diffusion imaging of human intracranial tumours. Neuroradiology 1997; 39:483–489.
6. Le Bihan D, Douek P, Argyropoulou M, Turner R, Patronas N, Fulham M. Diffusion and perfusion magnetic resonance imaging in brain tumors. Top Magn Reson Imaging 1993; 5:25–31.
7. Tien RD, Felsberg GJ, Friedman H, Brown M, Macfall J. MR imaging of high-grade gliomas: value of diffusion-weighted echoplanar pulse sequences. AJR Am J Roentgenol 1994; 162:671–677.
8. Tsuruda JS, Chew WM, Moseley ME, Norman D. Diffusion-weighted MR imaging of extraaxial tumors. Magn Reson Med 1991; 19:316–320.
9. Yanaka K, Shirai S, Kimura H, Kamezaki T, Matsumura A, Nose T. Clinical application of diffusion-weighted magnetic resonance imaging to intracranial disorders. Neurol Med Chir 1995; 35:648–654.
10. Brunberg JA, Chenevert TL, McKeever PE, et al. In vivo MR determination of water diffusion coefficients and diffusion anisotropy: correlation with structural alteration in gliomas of the cerebral hemispheres. Am J Neuroradiol 1995; 16:361–371.
11. Niendorf T, Dijkhuizen RM, Norris DG, van Lookeren Campagne M, Nicolay K. Biexponential diffusion attenuation in various states of brain tissue: implications for diffusion-weighted imaging. Magn Reson Med 1996; 36:847–857.
12. Mulkern RV, Gudbjartsson H, Westin CF, et al. Multi-component apparent diffusion coefficients in human brain. NMR Biomed 1999; 12:51–62.
13. Gudbjartsson H, Maier SE, Mulkern RV, Morocz IA, Patz S, Jolesz FA. Line scan diffusion imaging. Magn Reson Med 1996; 36:509–519.
14. Maier SE, Gudbjartsson H, Patz S, et al. Line scan diffusion imaging: characterization in healthy subjects and stroke patients. AJR Am J Roentgenol 1998; 17:85–93.
15. Robertson RL, Maier SE, Robson CD, Mulkern RV, Karas PM, Barnes PD. MR line scan diffusion imaging of the brain in children. AJNR Am J Neuroradiol 1999; 20:419–425.
16. Basser PJ, Pierpaoli C. A simplified method to measure the diffusion tensor from seven MR images. Magn Reson Med 1998; 39:928–934.
17. Le Bihan D. Molecular diffusion nuclear magnetic resonance imaging. Magn Reson Q 1991; 7:1–30.
18. Turner R, Le Bihan D, Maier J, Vavrek R, Hedges LK, Pekar J. Echo-planar imaging of intravoxel incoherent motions. Radiology 1990; 177:407–414.
19. Haselgrove JC, Moore JR. Correction for distortion of echo-planar images used to calculate the apparent diffusion coefficient. Magn Reson Med 1996; 36:966–964.
20. Le Bihan D, Breton E, Lallemand D, Aubin ML, Vignaud J, Laval-Jeantet M. Separation of diffusion and perfusion in intravoxel incoherent motion MR imaging. Radiology 1988; 168:497–505.
21. Conturo TE, McKinstry RC, Aronovitz JA, Neil JJ. Diffusion MRI: precision, accuracy and flow effects. NMR Biomed 1995; 8:307–332.
22. Warach S, Chien D, Li W, Ronthal M, Edelman RR. Fast magnetic resonance diffusion-weighted imaging of acute stroke. Neurology 1992; 42:1717–1723.
23. Mulkern RV, Zengingonul HP, Robertson RL, et al. Multi-component apparent diffusion coefficients in human brain: relationship to spin-lattice relaxation. Magn Reson Med 2000; 44:292–300.
24. Hajnal JV, Doran M, Hall AS, et al. MR imaging of anisotropically restricted diffusion of water in the nervous system: technical, anatomic, and pathologic considerations. J Comput Assist Tomogr 1991; 15:1–18.
25. Neeman M, Jarret KA, Sillerud LO, Freyer JP. Self-diffusion of water in multicellular spheroids measured by magnetic resonance microimaging. Cancer Res 1991; 51:4072–4079.
26. Pilatus U, Shim H, Artemov D, Davis D, van Zijl PCM, Glickson JD. Intracellular volume and apparent diffusion constants of perfused cancer cell cultures, as measured by NMR. Magn Reson Med 1997; 37:825–832.
27. Sevick RJ, Kanda F, Mintorovitch J, et al. Cytotoxic brain edema: assessment with diffusion-weighted MR imaging. Radiology 1992; 185:687–690.
28. van Zijl PCM, Moonen CTW, Faustino P, Pekar J, Kaplan O, Cohen JS. Complete separation of intracellular and extracellular information in NMR spectra of perfused cells by diffusion-weighted spectroscopy. Proc Natl Acad Sci USA 1991; 88:3228–3232.
29. Morriss C, Haselgrove J. Intravenous gadolinium does not alter the apparent diffusion coefficient: a study in enhancing brain tumors (abstr). In: Proceedings of the Eighth Meeting of the International Society for Magnetic Resonance in Medicine. Berkeley, Calif: International Society for Magnetic Resonance in Medicine, 2000; 1103.